Available online at www.sciencedirect.com
SCIENCE DIRECT
Journal of Sound and Vibration 294 (2006) 97–124
JOURNAL OF SOUND AND VIBRATION
www.elsevier.com/locate/jsvi

Structural health monitoring using empirical mode decomposition and the Hilbert phase

Darryll Pines[a,*], Liming Salvino[b]

[a]*Smart Structures Laboratory, Alfred Gessow Rotorcraft Center, University of Maryland, College Park, MD 20742, USA*
[b]*Structures and Composites (Code 652), Carderock Division, Naval Surface Warfare Center, West Bethesda, MD 20817, USA*

Received 23 May 2003; received in revised form 7 October 2005; accepted 25 October 2005
Available online 30 January 2006

Abstract

This paper discusses a new signal processing tool involving the use of empirical mode decomposition and its application to health monitoring of structures. Empirical mode decomposition is a time-series analysis method that extracts a custom set of basis functions to describe the vibratory response of a system. In conjunction with the Hilbert Transform, the empirical mode decomposition method provides some unique information about the nature of the vibratory response. In this paper, the method is used to process time-series data from a variety of 1-D structures with and without structural damage. Empirically derived basis functions are processed through the Hilbert–Huang Transform to obtain magnitude, phase, and damping information. This magnitude, phase, and damping information is later processed to extract the underlying incident energy propagating through the structure. This incident energy is also referred to as the dereverberated response of a structure. Using simple physics-based models of 1-D structures, it is possible to determine the location and extent of damage by tracking phase properties between successive degrees of freedom. This paper also presents experimental validation of this approach using a civil building model. Results illustrate that this new time-series method is a powerful signal processing tool that tracks unique features in the vibratory response of structures.

1. Introduction—advanced diagnostic methods

In recent years, there have been an extensive amount of research associated with the development of health monitoring methods for simple and complex mechanical, civil and aerospace systems, including buildings, elevator systems, and aerospace systems such as aging aircraft and rotorcraft. For many of these applications a complete framework for health monitoring of these systems is still evolving. Thus, there are a number of critical elements that are essential to successful application of robust structural health monitoring systems. These include elements such as the choice of sensors, electronics and software. At the core of this framework are the diagnostic and prognostic signal processing algorithms used to detect the presence, magnitude and extent of structural damage. The emergence of this field has led to a variety of on-line and off-line diagnostic methods for detecting, locating and quantifying varying degrees of damage. For structural components, these

*Corresponding author. Tel.: +1 301 405 0263; fax: +1 301 314 9011.
E-mail address: djpterp@eng.umd.edu (D. Pines).

0022-460X/$ - see front matter © 2006 Elsevier Ltd. All rights reserved.
doi:10.1016/j.jsv.2005.10.024

diagnostic techniques might be classified into four broad categories: (1) modal-based methods; (2) local diagnostic methods; (3) non-parametric methods, "blackbox"; (4) time-series/non-stationary methods.

With respect to modal methods, numerous researchers have developed analytical and experimental damage detection algorithms using experimentally measured mode shapes and natural frequencies [1]. However, modal techniques have not been widely accepted for practical structural systems, because of their sensitivity to sensor spacing, environmental effects (temperature, moisture), nonlinearities and boundary conditions. To counter many of these pitfalls, local diagnostic methods using piezoelectric sensors/actuators have evolved to improve sensitivity to local failure modes. These techniques rely on being in close proximity to structural damage and typically require many sensors distributed throughout a structure to achieve acceptable performance. Similar to conventional non-destructive evaluation methods, these local structural diagnostic methods tend to be qualitative in nature, especially in the high-frequency domain (>20 kHz). Typically, a damage index is developed to infer the presence and type of damage, as well as track increases in the amount of damage. Similar to modal methods, local diagnostic techniques also suffer from environmental effects, structural nonlinearities and high sensor density. Non-parametric methods such as neural networks and ARMA models have evolved to overcome the problems associated with environmental changes and system nonlinearities. Typically, statistical averaging is used to obtain mean characteristics of the signal response from a structure. By improving on local methods, this leads to a qualitative monitoring approach that is robust to environmental effects since statistical averaging is used to obtain mean representations of structures with and without damage. However, it becomes difficult to quantify damage without a physics-based coupling to the non-parametric parameters. The use of time-series analysis/non-stationary processing coupled with local physics-based models of structures is receiving increasing attention in the field of health monitoring. Time-series analysis such as the wavelet approach permit vibration signals from structures to be decomposed into fundamental basis functions that are used to characterize the vibration response. By tracking changes in these fundamental basis functions, it is possible to detect structural defects through inspection of time–frequency properties of the vibration signal.

Recently, a new time-series method has been developed to analyze nonlinear and non-stationary data [2]. A key property of the method is the extraction of "intrinsic mode functions" that admit well-behaved Hilbert Transforms in magnitude and phase. This approach is adaptive and lends itself to any time-series. When coupled with the Hilbert Transform, the "intrinsic mode functions" yield instantaneous frequencies as functions of time that give sharp identification of fundamental properties of vibration signals. For instance, instantaneous frequency, amplitude and damping can be extracted. In this paper, this information is used to track the damage in simple 1-D structures, including a scaled civil building testbed. The next section reviews the state of the art in spectral analysis of vibration data.

2. Spectral analysis of vibration data

2.1. Time-domain analysis

Prior to the discovery of the FFT and the implementation of the first real-time spectral analyzers, vibration analysis was predominantly performed by looking at details of the time-domain waveform of the signal. Although this enabled rudimentary detection and diagnosis of faults by examining the major repetitive components of a signal, complex signals with a multitude of components could not be accurately assessed. This lead to the emergence of several techniques that can be used to enhance the characteristics that are otherwise not readily observable from the time waveform. These include time-synchronous averaging, and auto-correlation of the signal. Time synchronous averaging uses the average of the signal over a large number of cycles, synchronous to the running speed of the machine. This attenuates any contributions due to noise or non-synchronous vibrations. The auto-correlation function is the average of the product. Application of the auto-correlation function on the time series allows us to indirectly obtain information about the frequencies present in the signal. However, these techniques only provide a limited amount of additional information. The need to distinguish between components of a similar nature or hidden within a complex vibration signal led to the mathematical representation of these signals in terms of their orthogonal basis functions, a field of mathematics whose origins date back to investigations into the properties of heat transfer.

2.2. Frequency-domain analysis

The advent of the Fourier Series in the early 1800s by Joseph Fourier (1768–1830) provided the foundations for modern signal analysis, as well as the basis for a significant proportion of the mathematical research undertaken in the 19th and 20th centuries. Fourier introduced the concept that an arbitrary function, even a function which exhibits discontinuity's, could be expressed by a single analytical expression. For a continuous function of period T, the Fourier series is given by

$$f(t) = \frac{a_o}{2} + \sum\left(a_n \cos\left(\frac{n\pi}{T}t\right) + b_n \sin\left(\frac{n\pi}{T}t\right)\right), \tag{1}$$

where the Fourier coefficients are calculated by

$$a_n = \frac{1}{T}\int F(t)\cos\left(\frac{n\pi t}{T}\right)\mathrm{d}t, \tag{2}$$

$$b_n = \frac{1}{T}\int F(t)\sin\left(\frac{n\pi t}{T}\right)\mathrm{d}t. \tag{3}$$

The coefficients of these orthonormal basis functions represent the contribution of the sine and cosine components of the signal at all frequencies. This allows the signal to be analyzed in terms of its frequency components. Despite the functionality of the Fourier transform, especially in regard to obtaining the spectral analysis of a signal, there are several shortcomings of this technique. The first of these is the inability of the Fourier transform to accurately represent functions that have non-periodic components that are localized in time or space, such as transient impulses. This is due to the Fourier transform being based on the assumption that the signal to be transformed is periodic in nature and of infinite length. Another deficiency is its inability to provide any information about the time dependence of a signal, as results are averaged over the entire duration of the signal. This is a problem when analyzing signals of a non-stationary nature, where it is often beneficial to be able to acquire a correlation between the time and frequency domains of a signal. This is often the case when monitoring mechanical vibrations.

A variety of alternative schemes have been developed to improve the description of non-stationary vibration signals. These range from developing mathematical models of the signal, to converting the signal into a pseudo-stationary signal through angular sampling, and time–frequency analysis of the vibrations.

2.3. Time–frequency signal analysis

As noted by Ville in 1947 [3] there are two basic approaches to time–frequency analysis. The first approach is to initially cut the signal into slices in time, and then to analyze each of these slices separately to examine their frequency content. The other approach is to first filter different frequency bands, and then cut these bands into slices in time and analyze their energy content. The first of these approaches is used for the construction of the short-time Fourier transform and the Wigner–Ville transform, while the second leads to discussions involving the wavelet transform. The wavelet transform is a mechanism used to separate a signal into its constituent parts, thus enabling analysis of data in different frequency domains with each components resolution matched to its scale. Alternatively, this may be seen as a decomposition of the signal into its set of basis functions (wavelets), analogous to the use of sines and cosines in Fourier analysis to represent other functions. These basis functions are obtained from dilations or contractions (scaling), and translations of the mother wavelet. The important difference that distinguishes the wavelet transform from Fourier analysis is its time and frequency localization properties. When analyzing signals of a non-stationary nature, it is often beneficial to be able to acquire a correlation between the time and frequency domains of a signal. In contrast to the Fourier transform, the wavelet transform allows localization in both the time domain via translations of the mother wavelet, and in the scale (frequency) domain via dilations. Although the wavelet transform has come into prominence during the last decade, the founding principles behind wavelets can be traced back as far as 1909 when Alfred Haar [4] discovered another orthonormal system of functions, such that for any

continuous function $f(t)$, the series

$$f(t) = \sum\sum a_{2^j+k} w(2^j t - k), \quad 0 \leqslant t < 1 \tag{4}$$

converges to $f(t)$ uniformly over the interval. Haar's research led to the simplest of the orthogonal wavelets, a set of rectangular basis functions depicted in Fig. 1. The Haar basis function was of limited use due to it being discontinuous in nature. Further advancements in wavelet theory involved the introduction of the dyadic block by Littlewood and Paley. The dyadic block is a sequence of operators that act essentially as a bank of band pass filters with an interval of separation of approximately an octave. This allows us to rewrite the Fourier series in terms of its dyadic blocks,

$$\Delta_j f(t) = \sum (a_k \cos(kt) + b_k \sin(kt)), \tag{5}$$

$$f(t) = \frac{a_o}{2} + \sum \varepsilon \Delta_j f(t). \tag{6}$$

However, it was not until 1946 that the first time–frequency wavelets (Gabor wavelets) were introduced by Dennis Gabor [5], an electrical engineer researching communication theory. Gabors idea was to break a wave up into segments, and then analyze the individual segments of the wave (wavelets), each of which had a well-defined frequency band and position in time. Although, Gabor's wavelets worked for continuous decompositions of signals they were limited in their usefulness as corresponding wavelets for discrete systems did not exist. Shortly after Gabor's work, Ville [3] proposed another approach for obtaining a mixed signal representation. Ville's work was tied into the research of Wigner (1932), a physicist working in the field of

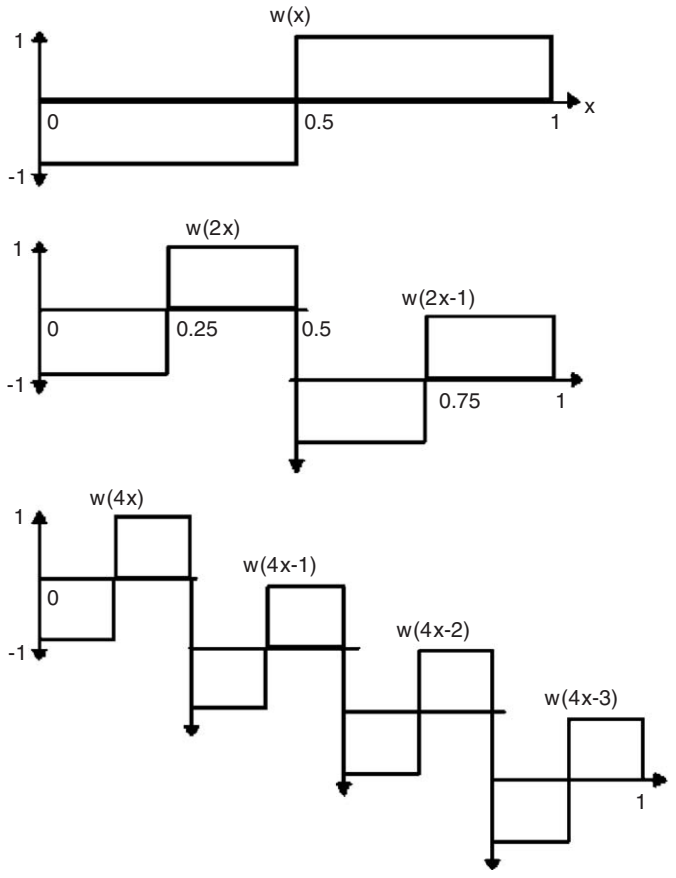

Fig. 1. Haar wavelets, 0, 1, 2 levels.

quantum mechanics, and led to the development of the Wigner–Ville transform, given by

$$W(\omega,t)=\int f(t+\tau/2)f^{*}(t-\tau/2)\mathrm{e}^{-\mathrm{j}\omega\tau}\,\mathrm{d}\tau,\quad 0\leqslant t<1, \tag{7}$$

where $f(t)$ is the original time signal. Unfortunately, the Wigner–Ville transform renders imperfect information about the energy distribution of the signal in the time–frequency domain, and an atomic decomposition of a signal based on the Wigner–Ville transform does not exist. Following from this work Yves Meyer, a mathematician researching into harmonic analysis, developed a family of wavelets that he showed to be the most efficient for modelling complex phenomena. The final transition from continuous signal processing to discrete signal processing was achieved by Daubechies [6,7] of Bell Labs and Mallat [8]. Since this work there has been a proliferation of activity with comprehensive studies expanding on the wavelet transform and its implementation into many fields of endeavor. Applications that have been explored include multi-resolution signal processing, image and data compression, telecommunications, fingerprint analysis, numerical analysis, speech processing and structural dynamics [9,10].

As compared to the Fourier transform, the wavelet transform and its derivatives offer significantly greater flexibility in the analysis of vibration data. Specifically, wavelet analysis represents a signal using a set of non-stationary waveforms (a wavelet dictionary), allowing non-stationary signals to be analyzed more effectively. Since many rotating machinery vibrations are at best quasi-stationary, wavelet analysis seems well suited to the problem of vibration-based diagnostics. Typical wavelet-based diagnostic algorithms tend to use the classical wavelet dictionaries that have been developed over the years for obtaining signal representations in over-complete dictionaries (e.g. Method of Frames, Matching Pursuit [11], High-Resolution Pursuit [12], Basis Pursuit [13]) over the possibility of using multiple dictionaries simultaneously for vibration-based diagnostics. In an over-complete dictionaries some elements may have representations in terms of these elements and as a consequence, any given signal representation is non-unique. Thus, the representation is referred to as adaptive, since there is the option of choosing the representation that best suits the application.

However, a disadvantage of current wavelet-based diagnostic algorithms is the use of currently available wavelet dictionaries. These dictionaries are not necessarily appropriate for analyzing rotating machinery vibrations. It has been proposed that a wavelet system that shapes itself to the signal under consideration could be more robust and useful in classification problems. The adapted lifting algorithm [14–16] uses properties of a given signal to create a dictionary suited to that particular signal. This adaptation property enables the creation of a general diagnostic algorithm that is able to tailor itself to a specific transmission, thus potentially enhancing sensitivity to damage. Samuel and Pines [17] have shown the use of this methodology for Helicopter transmission fault detection. The approach works well for faults that can be customized to the library of basis functions used in the adapted lifting algorithms. However, there still is a need for a new and more adaptive algorithm to identify faults in time-series data. In the next section, we introduce the concept of empirical mode decomposition as a new non-stationary time-series approach for analyzing time-domain vibration data.

3. Empirical mode decomposition

The empirical mode decomposition method [2] relies on generating a collection of intrinsic mode functions of a vibration signal.

3.1. Intrinsic mode functions—IMF

According to Huang, an intrinsic mode is a function that satisfies two conditions: (1) in the whole data set, the number of extrema and the number of zero crossings must either equal or differ at most by one; and (2) at any point, the mean value of the envelope defined by the local maxima and the envelope defined by the local minima is zero. The name intrinsic mode is used to refer to the oscillation modes embedded in the vibration data. Thus, the IMF in each cycle involves only one mode of oscillation. An IMF is not restricted to narrow band signals, and it can be both amplitude and frequency modulated.

3.2. Sifting process

Having defined the concept of an intrinsic mode function, we have to divide the vibration signal into its family of intrinsic modes. This process is known as decomposition and is based on several assumptions. Firstly, the signal must have at least two extrema, one maximum and one minimum; secondly, the characteristic time scale is defined by the time lapse between the extrema; and thirdly, if the data were totally devoid of extrema, but contained inflection points, then the signal could be differentiated one or more times to reveal the extrema. Final results can be obtained by integrating all components. Thus, essential to applying this new method is obtaining the intrinsic oscillatory modes of a vibration signal. A schematic of the process to identify intrinsic modes of a signal is summarized in Fig. 2. By virtue of the IMF definition, the decomposition method can simply use the envelopes defined by the local maxima and minima separately. Once the extrema are identified, all the local maxima are connected by a cubic spline function to define the upper envelope curve, shown in Fig. 2. One simply has to repeat the procedure for the local minima to produce the lower envelope. The upper and lower envelopes should cover all the data between them.

The mean of the upper and lower extrema curves is designated as

$$X_{m_1}(t) = \frac{X_{\max} + X_{\min}}{2}. \tag{8}$$

Subtracting the mean from the original signal generates the first estimate of an intrinsic mode function

$$X(t) - X_{m_1}(t) = h_1. \tag{9}$$

This operation is named sifting which leads to the third curve displayed in Fig. 2. While h_1 represents a first estimate of the first intrinsic mode function, further sifting is usually needed. By performing successive siftings a better estimate of the first intrinsic mode function can be obtained. The next sifting assumes that h_1 is the signal so that the next estimate becomes

$$h_1 - X_{m11}(t) = h_{11}. \tag{10}$$

After k siftings we define the first intrinsic mode to be

$$c_1(t) = h_{1k}. \tag{11}$$

When performing the sifting process there are a number of issues to be concerned with, including the elimination of riding waves and the smoothing of uneven amplitudes. One must pay particular attention to performing too many siftings and creating spurious amplitudes that have no physical meaning. In addition, Huang points out that one must pay particular attention to cubic spline fittings near the boundaries. Thus, Huang defines a measure for terminating the sifting process by defining the standard deviation between to

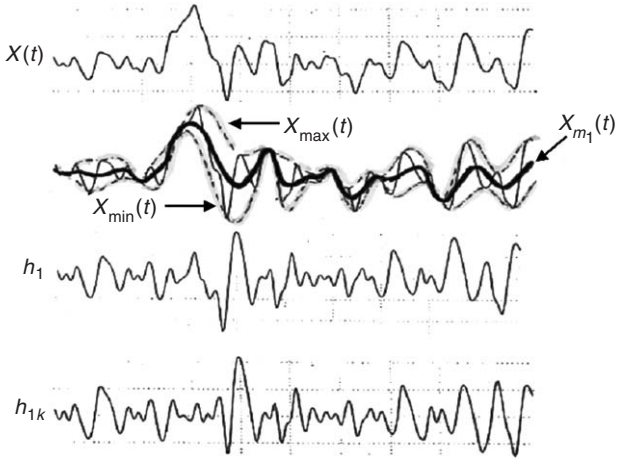

Fig. 2. Sifting process to obtain intrinsic mode functions.

successive siftings to be

$$\text{S.D.} = \sum \left[\frac{(h_{1(k-1)}(t) - h_{1k}(t))^2}{h_{1(k-1)}(t) * h_{1(k-1)}(t)} \right]. \tag{12}$$

Typical values of S.D. are 0.2 and 0.3. To obtain the second and subsequent intrinsic mode functions, the residual signal can be computed as

$$X(t) - c_1(t) = r_1(t). \tag{13}$$

The residual, r_1, now becomes the new data that can be subjected to the same sifting process to extract more intrinsic mode functions. This process is repeated to obtain c_2 through c_n intrinsic mode functions. By summing up all of the intrinsic mode functions it is possible to represent a vibration signal as

$$X(t) = \sum c_i(t) + r_n. \tag{14}$$

Thus, the original data $X(t)$ has been divided into n empirical modes, c_n, plus a residue, r_n.

3.3. Hilbert–Huang transform

Having obtained the intrinsic mode functions from the sifting process above, the Hilbert Transform is used to obtain phase and frequency. Thus, for a given IMF $c_i(t) \equiv C(t)$, the Hilbert Transform becomes

$$D(t) = \frac{1}{\pi} P \int \frac{C(t')}{t - t'} \, \mathrm{d}t'. \tag{15}$$

This implies that the analytic signal becomes

$$Z(t) = C(t) + \mathrm{i}D(t) = a(t)\mathrm{e}^{\mathrm{i}\theta(t)}, \tag{16}$$

where the amplitude and phase are given by

$$a(t) = \sqrt{C(t)^2 + D(t)^2}, \quad \theta(t) = \arctan\left(\frac{D(t)}{C(t)}\right). \tag{17,18}$$

Here the notion of phase angle refers to that of a trigonometric function. The IMF is a well-defined function for any time t with monotonically increasing values.

3.3.1. Instantaneous frequency and phase

The concept of frequency and phase has significant meaning when applying the intrinsic mode functions. If the IMFs can be considered to be strictly local, then instantaneous frequency can be defined as

$$\omega(t) = \frac{\mathrm{d}\theta(t)}{\mathrm{d}t}, \tag{19}$$

where θ is the phase obtained from the application of the Hilbert Transform to the intrinsic mode functions. Because the functions are restricted to have certain properties, the phase can be considered to be local and to increase monotonically as a function of time. This is only possible if the functions are restricted to be symmetrically local with respect to the mean zero level. This helps to avoid a number of paradoxes associated with the concept of the analytic signal, $Z(t)$ and phase. Some of these difficulties include the fact that (1) the instantaneous frequency may not be one of the frequencies in the spectrum; (2) the instantaneous frequency may be continuous and range over an infinite number of values; and (3) that for a band-limited signal, the instantaneous frequency may go outside of the band. Thus, to resolve many of these paradoxes when applying the concept of instantaneous frequency, properties of the intrinsic mode functions must be restricted.

3.3.2. Hilbert Spectrum

As explained in the above sections, Eq. (17,18) represents a well-defined phase function for any time t with monotonically increasing values. Therefore, its time derivatives should remain positive at all times. If an analytic signal is viewed as a rotation in the complex plane with radius of rotation $a(t)$ and instantaneous

phase angle $\theta(t)$, the instantaneous angular velocity of the rotation $\omega(t)$, or instantaneous frequency $f(t) = \omega(t)/2\pi$ should remain positive for all time t. This instantaneous frequency $f(t)$ is physically meaningful and can be used to construct the time–frequency spectrum $H(f,t)$, known as the Hilbert Spectrum or the Hilbert–Huang Transformation (HHT). $H(f,t)$ is constructed by generalization of ordered triplet $[t,f(t),a(t)]$ into a function of two variables $[t,f,H(f,t)]$ where $a(t) = H(f(t),t)$.

3.4. Damping

The damping or loss factor values can be calculated from the response data directly using the Hilbert Damping Spectrum [18,19]. The first step is to define a time-dependent decay factor for each empirical mode (or IMF) given in Eq. (16), which is rewritten as $Z(t) = a(t)e^{j\theta(t)} = Ce^{-\phi(t)+j\theta(t)}$. The time-dependent decay $\phi(t)$ is then defined by using

$$\frac{d\phi(t)}{dt} = \frac{1}{2}\gamma(t) = -\frac{\dot{a}(t)}{a(t)}. \tag{20}$$

If $\gamma(t) = \gamma$ is a constant, the infinite time integral of this function agrees with the basic decay envelope used in the conventional damping formulation ($\phi(t) = \frac{1}{2}\gamma t$). In the next step, dimensionless variables

$$\zeta(t) = \frac{\gamma(t)}{2\omega_0(t)} \quad \text{and} \quad \eta(t) = 2\zeta(t)$$

are formulated corresponding to the conventional critical damping ratio or damping loss factor. The variable $\eta(t)$ can be evaluated at a given time t and instantaneous system frequency $\omega(t)$, which is modeled by the EMD and Hilbert transform method as

$$\omega(t) = \sqrt{\omega_0(t)^2 - (\gamma(t)/2)^2}. \tag{21}$$

The final representation of time- and frequency-dependent damping is the quantity $\eta(t)$ for each IMF function contoured on the time and frequency plane. This is similar to the treatment of the Hilbert Spectrum introduced in Huang [2]. The term $\eta(\omega,t)$ is a time- and frequency-dependent damping loss factor, named the Hilbert Damping Spectrum.

$$\eta(\omega,t)^2 = \left(-\frac{2\dot{a}(\omega,t)}{a(\omega,t)}\right)^2 \left(\omega^2 + \left(\frac{\dot{a}(\omega,t)}{a(\omega,t)}\right)^2\right)^{-1}. \tag{22}$$

If the frequency-dependent damping is the only feature of interest and the system is linear, damping can be expressed as a function of ω only.

3.5. Example of time–frequency response

To illustrate properties of the intrinsic mode functions when coupled to the Hilbert Transform, lets apply the analysis developed above to a simple example. Consider the signal displayed in Fig. 3. Two sinusoids are displayed, one at high frequency and one at low frequency. A sharp change in the appearance of the two frequencies occurs at $t = 500$ s. The respective time–frequency representations of this signal are compared on a contour plot. Notice that the wavelet transform using Morlet basis functions has a tendency to smear the response, thus losing a substantial amount of resolution. However, the empirical mode decomposition method with marginal Hilbert–Huang spectrum delivers fine detail about the nature of the two simulated sine wave signals. There is little if any leakage and the frequencies appear as sharp lines in the time–frequency plot.

This detail can be seen in the 3-D plots of Fig. 4. A Fourier transform can identify two of the frequencies but without any time-domain information. Notice that the EMD plot is very sharp when compared with the smeared results of the Wavelet Transforms. This suggests that the EMD-Hilbert–Huang Transform is capable of providing a more crisp indication of the frequencies in the signal. This property will be used in the next section to characterize the incident and dereverberated wave response of a simple structure.

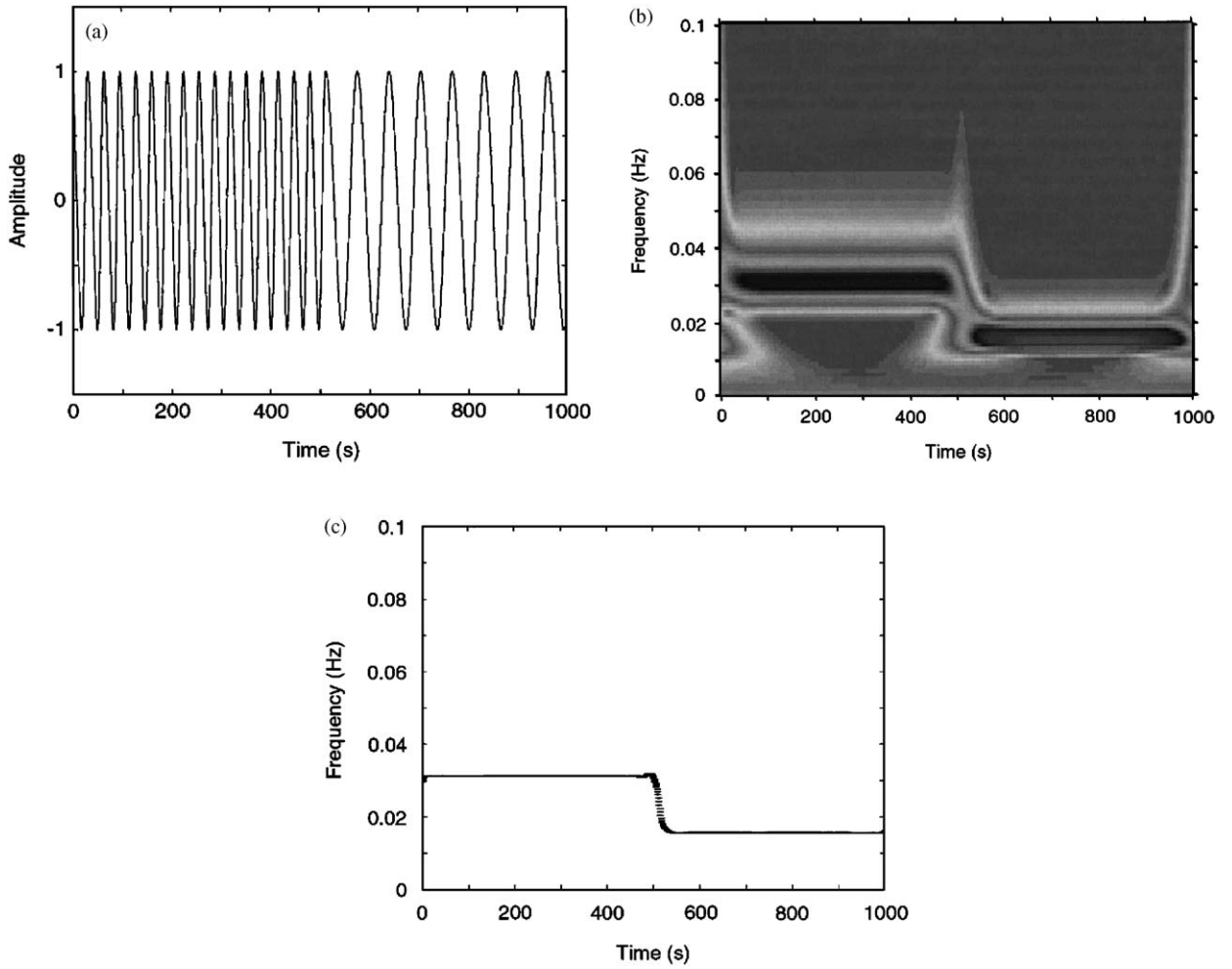

Fig. 3. Two sinusoid example: (a) time-domain function, (b) wavelet transform using Morlet basis functions, and (c) Hilbert–Huang spectrum.

4. Concept of dereverberation

4.1. Discrete 1-D structural elements

The concept of phase dereverberation of a structure can be interpreted as obtaining the response of a structure to the incident energy imparted to the system. By tracking how this energy migrates throughout a structure, it is possible to infer damage between two successive degrees of freedom [20,21]. The central idea is that as waves propagate through a structure, their speed changes if the local properties in the structure change. Thus, it is possible to infer damage by observing how the propagation delay between two points on a structure change over a particular frequency range.

To illustrate this concept consider the asymmetric element shown in Fig. 5. The equations of motion of this element can be represented by

$$\begin{bmatrix} k & -k \\ -k & k - m\omega^2 \end{bmatrix} \begin{bmatrix} W_L \\ W_R \end{bmatrix} = \begin{bmatrix} F_L \\ F_R \end{bmatrix}. \tag{23}$$

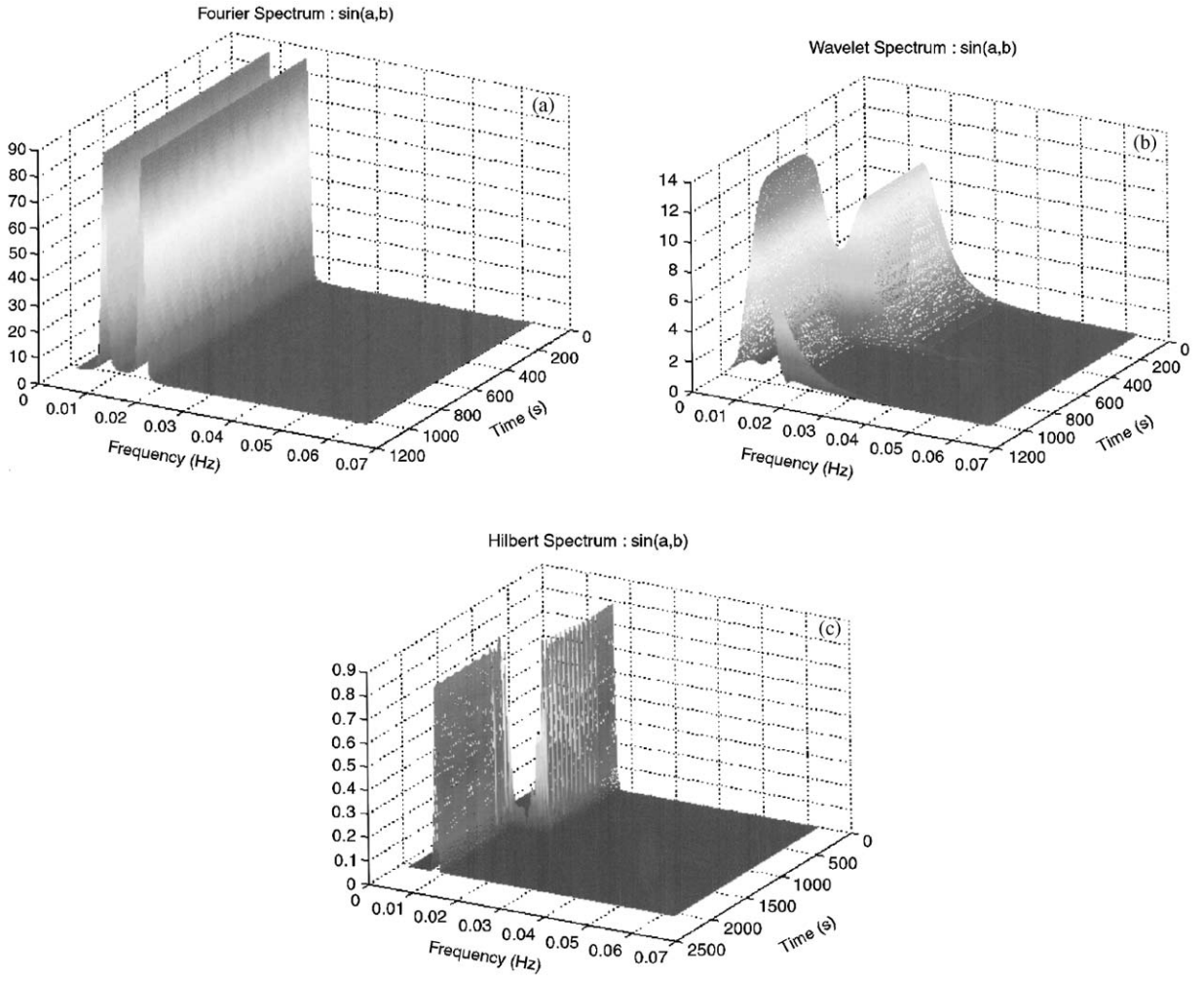

Fig. 4. Three-dimensional time–frequency representations: (a) Fourier spectrum, (b) wavelet spectrum, and (c) Hilbert spectrum.

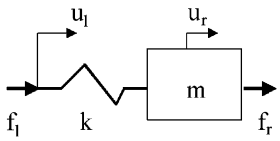

Fig. 5. Discrete asymmetric structural element.

After re-arrangement, Eq. (23) becomes

$$\begin{bmatrix} U_R \\ F_R \end{bmatrix} = \begin{bmatrix} 1 & -\dfrac{1}{k} \\ -m\omega^2 & \dfrac{k - m\omega^2}{k} \end{bmatrix} \begin{bmatrix} U_L \\ F_L \end{bmatrix} = T \begin{bmatrix} U_L \\ F_L \end{bmatrix}. \tag{24}$$

T is the transformation matrix and the wave propagation constant of this element is

$$\mu = \cosh^{-1}\left(\frac{2k - m\omega^2}{2k}\right) = \cosh^{-1}\left(\frac{T_{11} + T_{22}}{2}\right), \tag{25}$$

where $T_{22}=1$, $T_{22}=(k-m\omega^2)/k$ are diagonal elements of transformation matrix T. An eigenvalue problem can be formulated as $(\lambda I-T)\bar{\phi}=0$. By solving this equation, eigenvalues of transformation matrix T can be obtained as $\lambda_1=e^{\mu}$ and $\lambda_2=e^{-\mu}$. The λ_1 term corresponds to left propagating wave component W_{LP} while λ_2 corresponds to right propagating wave component W_{RP}. The two eigenvectors are $[\phi_{11}\ \phi_{12}]^{\mathrm{T}}=[1\ k(1-e^{-\mu})]^{\mathrm{T}}$ and $[\phi_{21}\ \phi_{22}]^{\mathrm{T}}=[1\ k(1-e^{\mu})]^{\mathrm{T}}$. The state vector $[U_L\ F_L]^{\mathrm{T}}$ can be uniquely decomposed in the wave coordinate space spanned by these two eigenvectors. The state vectors of this asymmetric element can be represented as

$$\begin{bmatrix} U_L \\ F_L \end{bmatrix} = \begin{bmatrix} 1 & 1 \\ k(1-e^{-\mu}) & k(1-e^{\mu}) \end{bmatrix} \begin{bmatrix} W_{\mathrm{LP}}(0) \\ W_{\mathrm{RP}}(0) \end{bmatrix}, \tag{26}$$

$$\begin{bmatrix} U_R \\ F_R \end{bmatrix} = \begin{bmatrix} 1 & 1 \\ k(e^{-\mu}-1) & k(e^{\mu}-1) \end{bmatrix} \begin{bmatrix} W_{\mathrm{LP}}(L) \\ W_{\mathrm{RP}}(L) \end{bmatrix}. \tag{27}$$

For the asymmetric element shown in Fig. 5, energy is assumed to be input from the left with $F_L=0$. A controller can be added at the right end to extract energy out. The control force is designed to have the form $F_c=GU_R=GW_{\mathrm{LP}}(L)+GW_{\mathrm{RP}}(L)$ and must satisfy two objectives: (1) equilibrium of forces at degree of freedom U_R, and (2) prevent energy reflection from the right end. Therefore, the control force, F_c, must satisfy the equations:

$$F_R+F_C=0, \quad W_{\mathrm{LP}}(L)=0. \tag{28}$$

By imposing $W_{\mathrm{LP}}(L)=0$, the frequency-dependent control gain is determined to be

$$G=k(1-e^{-\mu}). \tag{29}$$

If the reverberated transfer function (RTF) matrix of an asymmetric element is given by

$$\mathrm{RTF}=\begin{bmatrix} \dfrac{U_L}{F_L} \\ \dfrac{U_R}{F_L} \end{bmatrix} = \begin{bmatrix} k & -k \\ -k & k-m\omega^2 \end{bmatrix}^{-1}, \tag{30}$$

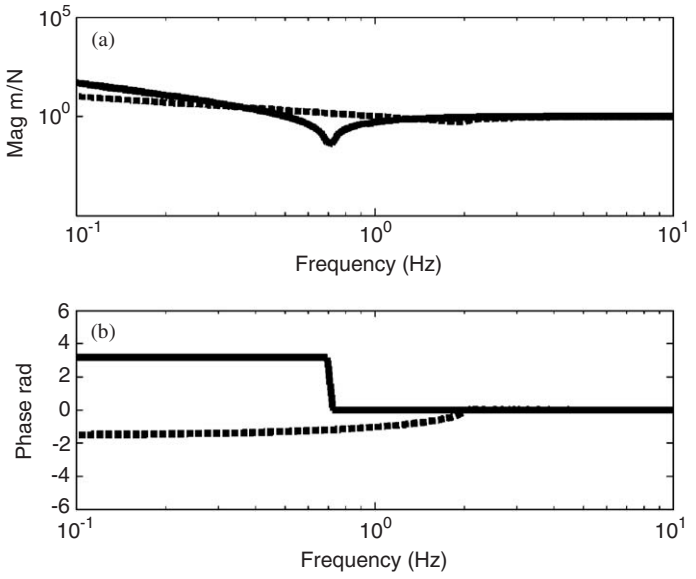

Fig. 6. RTF and DTF of U_L: ——, U_L/F_L; – –, $(U_L/F_L)_{\mathrm{DTF}}$; (a) magnitude and (b) phase.

dereverberated transfer functions (DTFs) U_L/F_L and U_R/F_L can be obtained using the expression

$$\begin{bmatrix} \dfrac{U_L}{F_L} \\ \dfrac{U_R}{F_L} \end{bmatrix} = \left(\mathrm{RTF}^{-1} + \begin{bmatrix} 0 & 0 \\ 0 & G \end{bmatrix} \right)^{-1} \begin{bmatrix} 1 \\ 0 \end{bmatrix}. \tag{31}$$

The RTF and DTF responses of U_L/F_L and U_R/F_L are shown in parts of Figs. 6 and 7, respectively. As expected the effect of the control force, F_c, is to remove the resonance, and anti-resonance from the response. The control gains for the asymmetric structural elements are plotted versus frequency in Fig. 8. Notice that

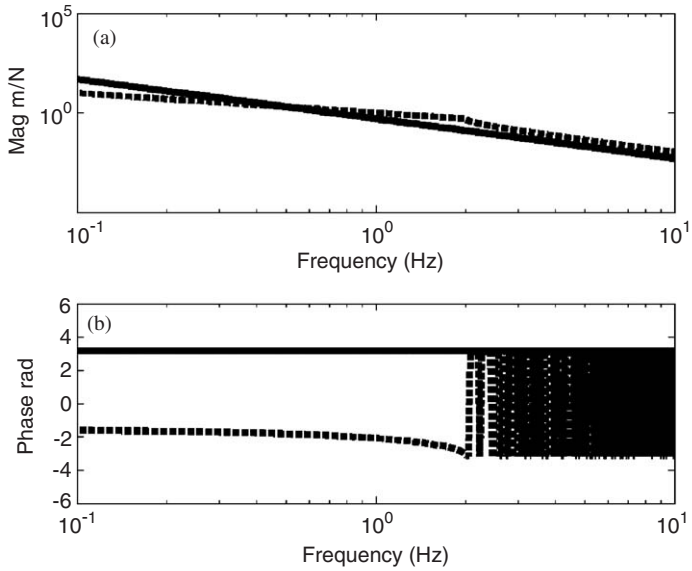

Fig. 7. RTF and DTF of U_R: ——, U_R/F_L; – –, $(U_R/F_L)_{\mathrm{DTF}}$; (a) magnitude and (b) phase.

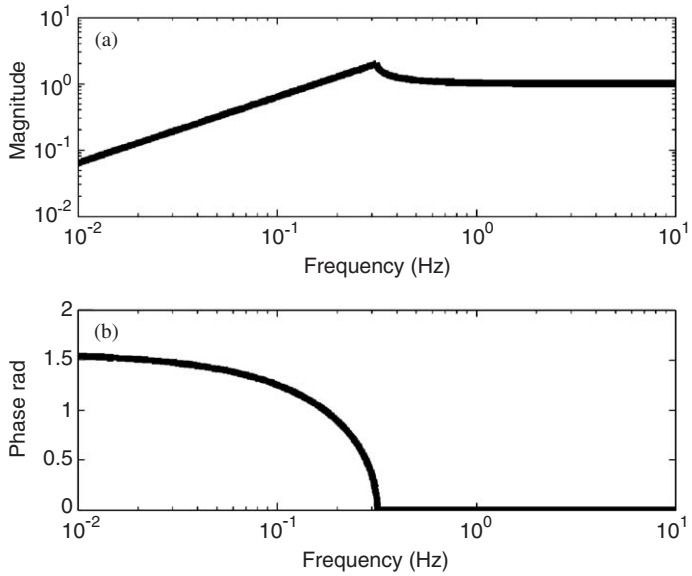

Fig. 8. Control gains, G, for asymmetric element: (a) magnitude and (b) phase.

this compensator has an unusual magnitude and phase behavior that is not consistent with conventional causal linear pole zero representations. The magnitude behavior for the compensator has a derivative type characteristic up until the cutoff frequency. However, the phase is not necessarily equal to 90°. Thus, such a compensator would be difficult to implement with conventional electronic components with these non-causal magnitude and phase properties. However, computationally these non-causal controllers can be implemented offline on analytical models of a structure simulated using a computer.

In addition to using a non-causal virtual controller to obtain the DTF response of a structure, the DTF response can also be obtained via analytical derivation. The DTF responses can be analytically expressed as

$$\frac{U_L}{F_L} = \frac{1}{k(1-\mathrm{e}^{-\mu})}, \quad \frac{U_R}{F_L} = \frac{\mathrm{e}^{-\mu}}{k(1-\mathrm{e}^{-\mu})}. \tag{32,33}$$

One important observation that can be made here is that the ratio of these two DTF responses is a pure phase lag term given by

$$\frac{U_R}{U_L} = \mathrm{e}^{-\mu}. \tag{34}$$

This DTF ratio is only dependent upon the structural properties enclosed by degrees of freedom U_R and U_L. Thus, it can be used to represent and track changes in the local structural dynamics.

4.2. Linear approximations

Table 1 compares the transmitted response ratio (U_R/U_L) of the asymmetric structural element for the reverberated, dereverberated and linear approximations of the DTFs. Closer inspection of Table 1 reveals that the transmitted displacement response ratio of the linearized DTF only depends upon the propagation parameter. This parameter is a function of localized mass and stiffness of the structure between degrees of freedom u_R and u_L. Thus, if a structure is damaged between two successive degrees of freedom, the DTF suggests that damage can be inferred by determining how this propagation parameter changes between two displacement measurements. Since μ is a complex frequency-dependent parameter, one simply has to examine the magnitude and phase of this parameter. In prior work, Pines and Ma [20] have shown that this parameter can be used to detect, locate and quantify the extent of damage by tracking the phase variations associated with the ratio (U_R/U_L).

4.3. EMD and phase dereverberation

Using the linearized expressions in Table 1, one can compare the phase relationships computed via wave propagation dereverberation methods and the phase computed from applying the Hilbert Transform and empirical mode decomposition. One goal is to ascertain any similarities between the phase computed in the time domain and the phase computed in the frequency domain using dereverberated wave mechanics. Below the cutoff frequency for the asymmetric discrete structural element, the phase delay between the response at U_R and U_L can be approximated as

$$\mathrm{phase}\left(\frac{U_R}{U_L}\right) = -\omega\sqrt{\frac{m}{2k}}. \tag{35}$$

Table 1
Transmitted response ratio (U_R/U_L)

RTF	DTF (nonlinear)	DTF (linear)
$\frac{U_L}{F_L} = \frac{k-m\omega^2}{-mk\omega^2}$	$\frac{U_L}{F_L} = \frac{1}{k(1-\mathrm{e}^{-\mu})}$	$\frac{U_L}{F_L} = \frac{1}{k\mu}$
$\frac{U_R}{F_L} = \frac{-1}{m\omega^2}$	$\frac{U_R}{F_L} = \frac{\mathrm{e}^{-\mu}}{k(1-\mathrm{e}^{-\mu})}$	$\frac{U_R}{F_L} = \frac{1-\mu}{k\mu}$
$\frac{U_R}{U_L} = \frac{-k/m}{k-m\omega^2}$	$\frac{U_R}{U_L} = \mathrm{e}^{-\mu}$	$\frac{U_R}{U_L} = 1-\mu \approx 1-\mathrm{j}\omega\sqrt{\frac{m}{2k}}$

To compare this expression to the Hilbert phase, let us consider the displacement response at the left degree of freedom to be given by

$$u_L(t) = A\ \sin(\omega_0 t). \tag{36}$$

Using the linear approximation of the structural dynamics between u_R and u_L, the DTF response at the right degree of freedom can be represented generically as

$$C(t) = u_R(t) = A\ \sin(\omega_0 t) - A\sqrt{\frac{m}{2k}}\omega_0\ \cos(\omega_0 t). \tag{37}$$

Computing the Hilbert Transform of u_R allows us to formulate the magnitude and phase as

$$D(t) = \frac{1}{\pi}\int \frac{U_R(t')}{t-t'}\,\mathrm{d}t'. \tag{38}$$

This leads to

$$D(t) = A\ \cos(\omega_0 t) - A\sqrt{\frac{m}{2k}}\omega_0 \sin(\omega_0 t). \tag{39}$$

Constructing the analytic function leads to

$$Z(t) = a(t)\mathrm{e}^{\mathrm{j}\theta(t)} = A\sqrt{1+\left(\omega_0^2\frac{m}{2k}\right)}\mathrm{e}^{\mathrm{j}(\omega_0 t+\omega_0\sqrt{m/2k})}. \tag{40}$$

Notice that the absolute value of the phase expression is identical to the phase derived for the DTF response. However, in the expression listed in Eq. (40) the phase is positive and increases with increasing time. Thus, for the linear approximation, it appears that the absolute value of the Hilbert phase is identical to the phase obtained from the dereverberated phase. This is important because it implies that one can perform all computations in the time domain and simply subtract the phase response between successive degrees of freedom to infer changes in local mass and stiffness properties. This approach will be illustrated below on a multi-dof example.

4.4. Magnitude and phase sensitivity to structural parameters

Eq. (40) summarizes the dependency of the magnitude and phase expressions for an intrinsic mode function on the structural parameters of a simple asymmetric structural element excited at a harmonic input frequency. Because one would like to infer structural damage using this representation of the intrinsic mode function, it is important to determine the sensitivity of these expressions to variations in structural parameters. This can be done by computing the derivative of $a(t)$ and $\theta(t)$ with respect to m and k, respectively. This leads to the following expressions for the magnitude and phase sensitivity with respect to structural parameters m and k:

$$\frac{\mathrm{d}a(t)}{\mathrm{d}m} = \frac{A(\omega_0^2/\omega_c^2)}{2m\sqrt{1+(\omega_0^2/\omega_c^2)}}, \quad \frac{\mathrm{d}a(t)}{\mathrm{d}k} = \frac{-A(\omega_0^2/\omega_c^2)}{2k\sqrt{1+(\omega_0^2/\omega_c^2)}}, \tag{41,42}$$

$$\frac{\mathrm{d}\theta(t)}{\mathrm{d}m} = \frac{-1}{2m}\frac{\omega_0}{\omega_c}, \quad \frac{\mathrm{d}\theta(t)}{\mathrm{d}k} = \frac{1}{2k}\frac{\omega_0}{\omega_c}, \tag{43,44}$$

where the frequency ratio is defined as

$$\omega_{\mathrm{nd}} = \frac{\omega_0}{\omega_c}, \quad \omega_c = \sqrt{\frac{2k}{m}}. \tag{45}$$

Fig. 9 plots the magnitude of the non-dimensional amplitude and phase sensitivity versus non-dimensional frequency ratio. This figure illustrates that below the cutoff frequency the phase expression has the greatest sensitivity to changes in structural parameters. Thus, it is anticipated that the phase expression would be a better indicator of damage in a simple (1-D) structure.

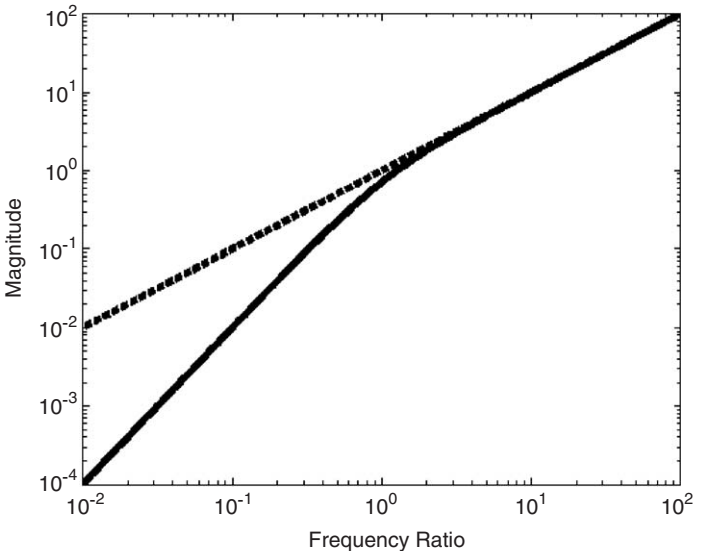

Fig. 9. Magnitude and phase sensitivity: ——, magnitude sensitivity; – –, phase sensitivity.

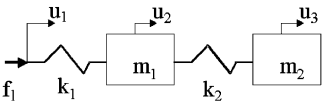

Fig. 10. Three-degree of freedom model.

5. Structural health monitoring using EMD

5.1. Multi-dof example

Consider the 3-dof spring-mass system displayed in Fig. 10. The equation of motion for this system is given generically by $M\ddot{x} + Kx = F$, where

$$M = \begin{bmatrix} 0 & 0 & 0 \\ 0 & m_1 & 0 \\ 0 & 0 & m_2 \end{bmatrix}, \quad K = \begin{bmatrix} k_1 & -k_1 & 0 \\ -k_1 & k_1 + k_2 & -k_2 \\ 0 & -k_2 & k_2 \end{bmatrix}, \quad F = \begin{bmatrix} 1 \\ 0 \\ 0 \end{bmatrix}. \tag{46–48}$$

The RTF response for each degree of freedom can be represented as

$$\begin{bmatrix} u_1/F_1 \\ u_2/F_1 \\ u_3/F_1 \end{bmatrix}_{\text{RTF}} = \begin{bmatrix} k_1 & -k_1 & 0 \\ -k_1 & k_1 + k_2 - m_1\omega^2 & -k_2 \\ 0 & -k_2 & k_2 - m_2\omega^2 \end{bmatrix}^{-1} \begin{bmatrix} 1 \\ 0 \\ 0 \end{bmatrix}. \tag{49}$$

Similarly, using the concept of virtual control, the DTFs can be determined to be

$$\begin{bmatrix} u_1/F_1 \\ u_2/F_1 \\ u_3/F_1 \end{bmatrix}_{\text{DTF}} = \begin{bmatrix} k_1 & -k_1 & 0 \\ -k_1 & k_1 + k_2 - m_1\omega^2 + G_1 & -k_2 \\ 0 & -k_2 & k_2 - m_2\omega^2 + G_2 \end{bmatrix}^{-1} \begin{bmatrix} 1 \\ 0 \\ 0 \end{bmatrix}, \tag{50}$$

where virtual controllers G_1 and G_2 are given by

$$G_1 = k_1(1 - \exp(-\mu_1)) - k_2(1 - \exp(-\mu_2)), \tag{51}$$

$$G_2 = k_2(1 - \exp(-\mu_2)), \tag{52}$$

where μ_1 and μ_2 are the propagation coefficients.

Now consider the parameters defined in Table 2 for this simple 3-dof freedom system. With this information it is possible to compute the baseline response of the discrete system to an impulse from the left side. The damaged cases are generated by reducing the spring constants by 25%, 50%, and 75% for each k_1 and k_2 separately.

5.2. Phase dereverberation

The concept of phase dereverberation of a 1-D structures can be interpreted as obtaining the response of the structure to the incident energy imparted to the system. Thus, assuming that an impulse is applied to the first degree of freedom, it is not difficult to determine the RTFs and DTFs as displayed in Figs. 11–13 as the baseline response. Notice that the (DTFs) do not contain the resonant pole/zero characteristics commonly found in typical transfer functions since all internal and external reflections are cancelled using controllers G_1 and G_2. The corresponding baseline displacement responses of the reverberated and dereverberated time series are displayed in Figs. 14 and 15, respectively. Careful inspection of the dereverberated time series of this simple structure reveals a phase lag associated with the incident impulsive wave as it traverses the structure from left to right. Hence, by computing the ratio of successive degrees of freedom, one can track the variation in structural properties through the relative phase relationship between each successive degree of freedom. This ratio is computed for the dereverberated response time series in Fig. 15 and displayed in the frequency

Table 2
Baseline parameters of 3-dof spring–mass model

m_1	m_2	k_1	k_2
1	1	1	2.5

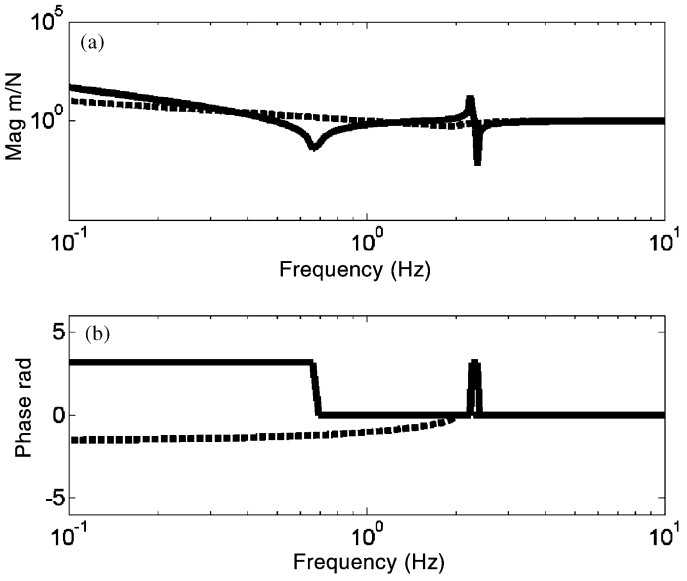

Fig. 11. RTF and DTF at u_1: ——, u_1/f_1; – –, $(u_1/f_1)_{\mathrm{DTF}}$; (a) magnitude and (b) phase.

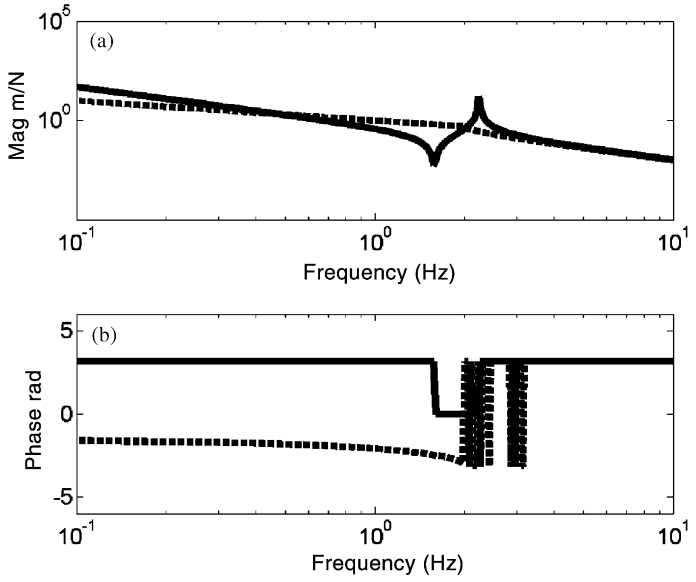

Fig. 12. RTF and DTF at u_2: ——, u_2/f_1; – –, $(u_2/f_1)_{\mathrm{DTF}}$; (a) magnitude and (b) phase.

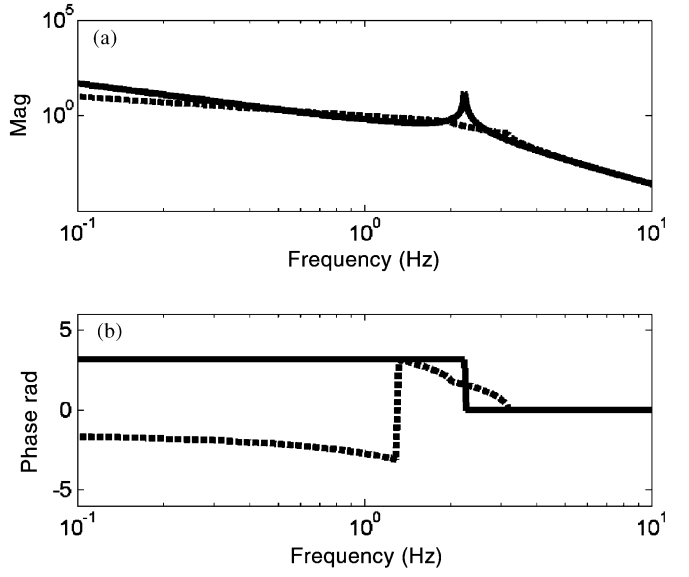

Fig. 13. RTF and DTF at u_3: ——, u_3/f_1; – –, $(u_3/f_1)_{\mathrm{DTF}}$; (a) magnitude and (b) phase.

domain in Fig. 16. Thus, as a structure becomes damaged, one would anticipate a change in these phase characteristics. An example of such a phase change for damage occurring in k_1 is given in Fig. 17. In previous work, tracking phase changes between successive degrees of freedom has been accomplished using a 'virtual controller', however, the use of Empirical Mode Decomposition permits this monitoring to involve only processing of the time-series data without the need for implementing a 'virtual controller'. Hence, by using the EMD approach the same relative phase information can be obtained to assess damage, shown in Fig. 18 between degrees of freedom u_1 and u_2. Fig. 18(a) shows the phase ratio for simulated damage in k_1. The comparisons are made for the baseline structure with three simulated damage cases (stiffness reduction of 25%, 50%, and 75%). the phase lags are clearly evident due to the softening spring. Fig. 18(b) shows the same

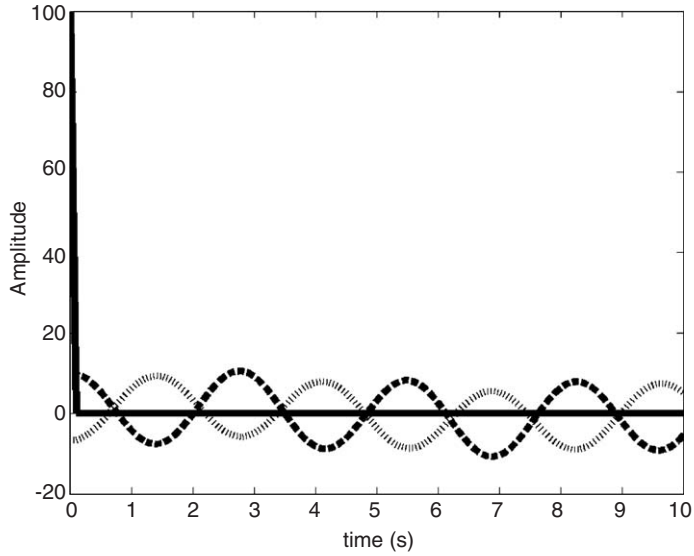

Fig. 14. Reverberant impulse response: ——, u_1; – –, u_2; ...., u_3.

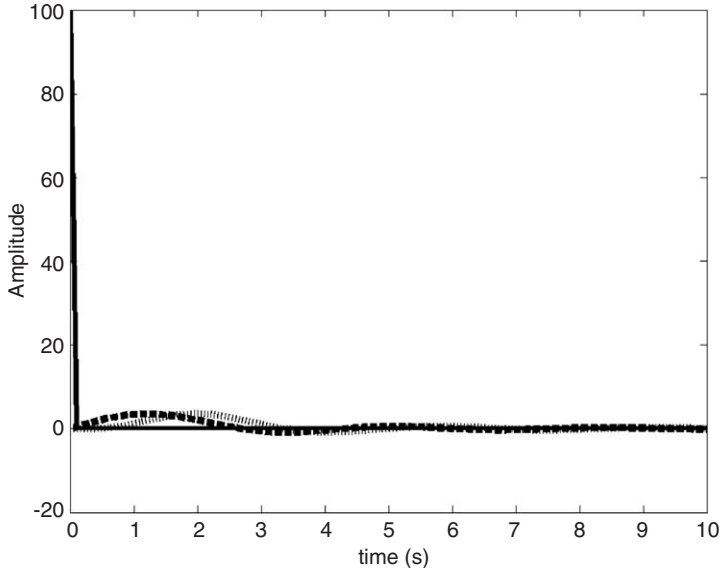

Fig. 15. Dereverberated impulse response: ——, u_1; – –, u_2; ...., u_3.

phase ratio for simulated damage in k_2. The phases remain constant for all damage cases because the damage occurring in k_2 (between degrees of freedom u_2 and u_3) does not affect the incident energy between degrees of freedom u_1 and u_2 for the dereverberated response.

6. Experimental validation

6.1. Civil building model

To evaluate the performance of the empirical mode decomposition method to aid in the detection and evaluation of structural damage, time-domain vibration data from a scaled civil building model was analyzed

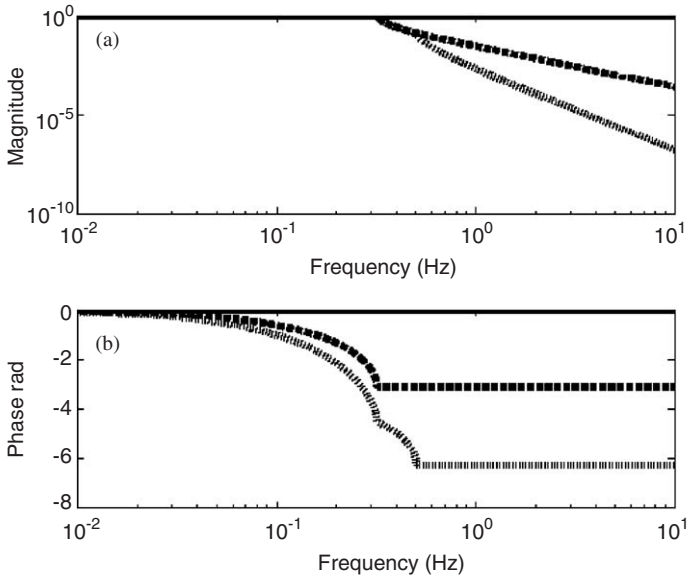

Fig. 16. Phase lag ratios—frequency domain (undamaged): ——, u_1/u_1; – –, u_2/u_1, ..., u_3/u_1; (a) magnitude and (b) phase.

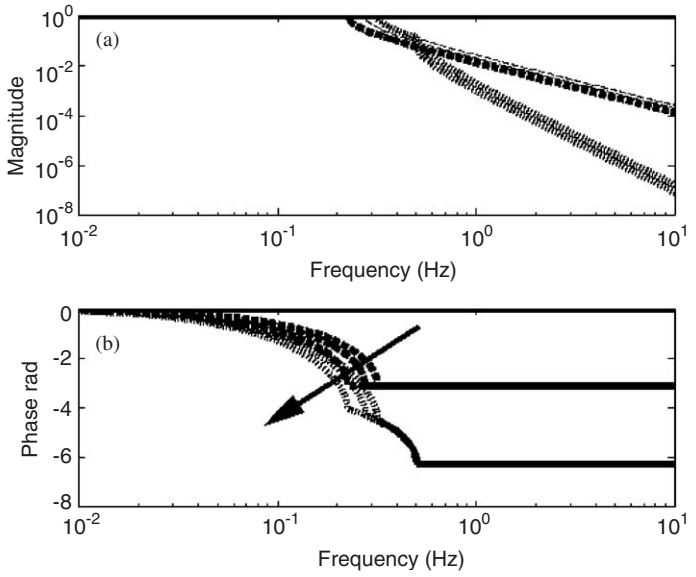

Fig. 17. Phase lag ratios—frequency domain (k_1 damaged): ——, u_1/u_1; – –, u_2/u_1; ...., u_3/u_1; (a) magnitude and (b) phase.

with and without the presence of damage. Results from this study are discussed below. The building model consisted of 3 stories with the ground floor driven by a hydraulic shake system, shown in Fig. 19. At each level a PCB accelerometers were mounted to measure the vibratory response of the building before and after damage. To simulate seismic loading, time series from the El Centro earthquake, shown in Fig. 20, was used as input to the hydraulic actuators. Notice that the undamaged natural frequencies were determined to be 2.5, 7, and 12 Hz, respectively, for the first three modes of the structure. Three damage cases were simulated by physically changing the properties of the structure. In the first two cases, stiffness damage was simulated by removing two bolts in the bottom flange near the ground level in case 1, and by removing two bolts from the third (top) floor connection in case 2. In case 3, one-third of the mass of the second floor was removed. The

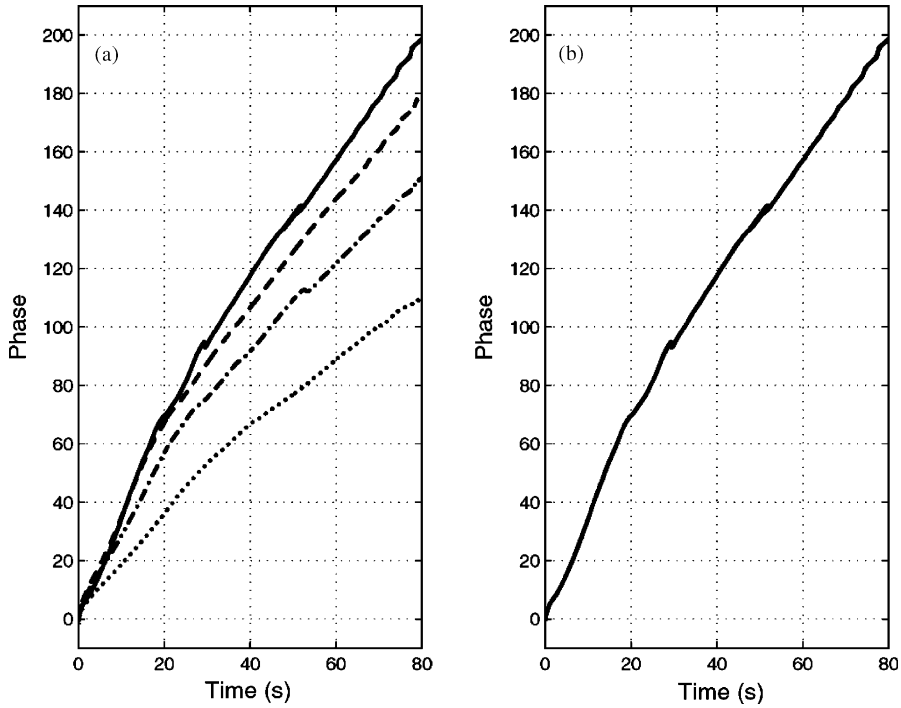

Fig. 18. Relative phases of dereverberated responses: ——, undamaged; – –, 25% damage; – · –; 50% damage; ...., 75% damage; (a) k_1 damage and (b) k_2 damage.

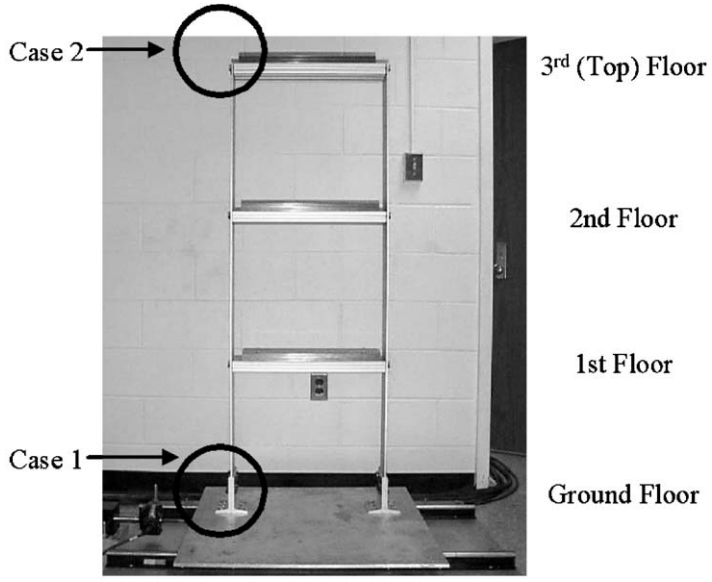

Fig. 19. Experimental building model.

time-series data obtained from all four accelerometers was processed through the empirical mode decomposition method to determine the presence, type and amount of damage. Results for cases 1 and 2 are discussed below.

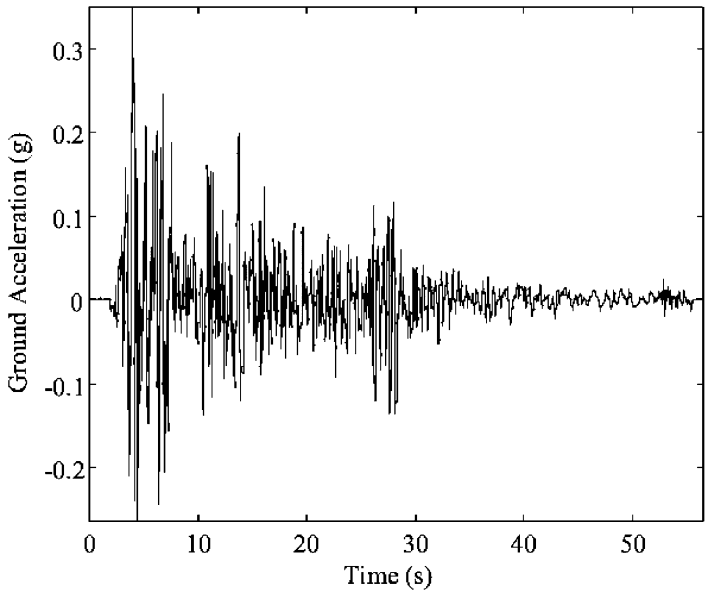

Fig. 20. El Centro forcing input.

6.1.1. Case 1: ground floor damage (two bolts loosened)

Fig. 21 displays the undamaged and damaged intrinsic mode functions of the ground floor acceleration for simulated damage between the ground floor and the first floor of the 3-dof building model. The second floor IMF plots are similar. In each case there are 9 derived intrinsic mode functions, but, in the figure, the lowest-frequency IMF is not shown. Careful inspection of these functions suggest that it is very difficult to ascertain the presence of damage in these time-domain decompositions. However, applying the Hilbert–Huang Spectrum reveals some unique features that appear in the time–frequency maps of the ground floor and second floor accelerometer signals plotted in Figs. 22 and 23, respectively. Notice the similarity in the time–frequency maps, $H(f,t)$, with the exception of the appearance of a noticeable distribution of broadband signal energy just before 3 s in the damaged amplitude map. This intensity is primarily due to the loosening of the bolts of the ground floor brace used to support the upper stories. As the seismic wave enters the ground floor the brace bangs against the loose bolts and vertical legs of the structure. This causes an impact to occur prior to the full seismic wave reaching the ground floor accelerometer. As the seismic wave continues to traverse up the building, a noticeable change starts to appear in the time–frequency response spectrum $H(f,t)$ displayed in Fig. 23. Notice that there is a significant loss in intensity between the undamaged and damaged responses. This is particularly true if one tracks the 3 modal frequency band of energy between the damaged and undamaged spectra. As the intensity in this frequency band diminishes, a new phenomena becomes apparent in the time–frequency response. At approximately 12 s, the third mode band start to spread as intensity decreases, suggesting the presence of a structural nonlinearity in the system caused by the loosening of the two bolts. This may be explained by the mating members becoming locked as the amplitude of vibration decreases. Fig. 24 confirms that this drop in intensity is consistent with an increase in damping in the system (second floor) as a result of members sliding back and forth against one another.

6.1.2. Case 2: third (top) floor damage (two bolts loosened)

Figs. 25 and 26 illustrate the case for simulated experimental damage in the third (top) floor corresponding to a stiffness loss caused by the loosening of two bolts. These figures plot the Hilbert–Huang spectrum, $H(f,t)$, for the second and third floor accelerometer signals. Notice that the effect of damage appears in both the second and third floor vibration signals. Each vibration signal contains three distinct characteristic bands of energy. Hence, the effect of damage in the top floor causes a slight shift in the mean bands and a spreading of the band. Moreover, inspection of these figures reveals that again the damping in the system has increased to

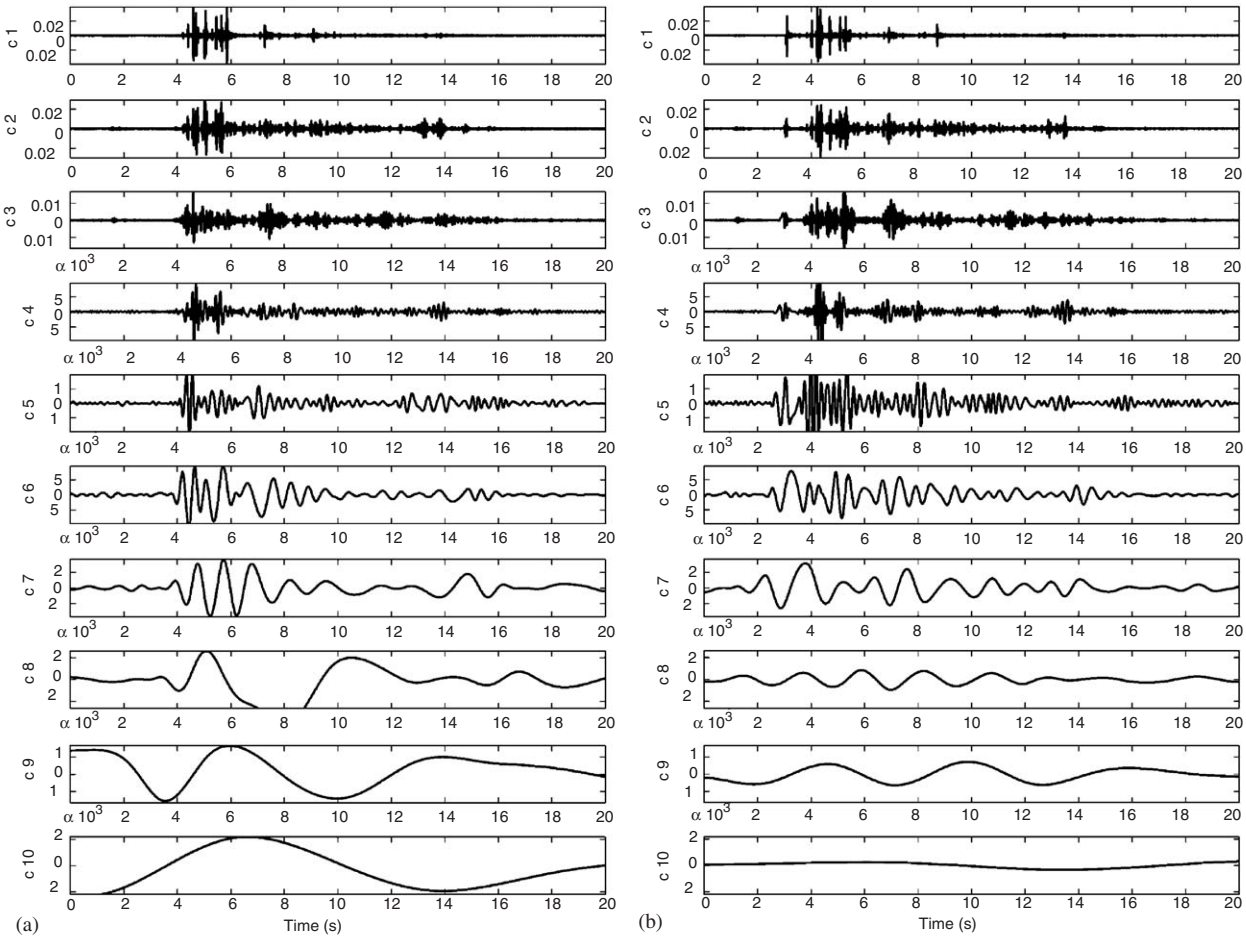

Fig. 21. Ground floor: intrinsic mode functions: (a) undamaged and (b) damaged.

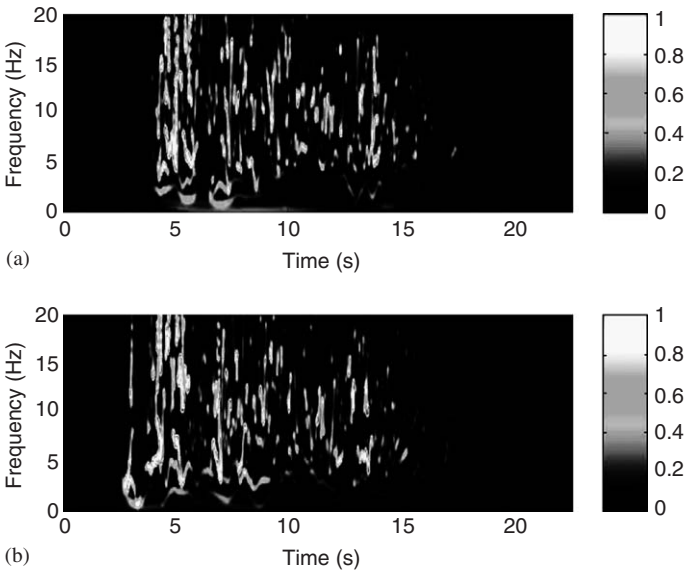

Fig. 22. Ground floor acceleration for ground floor damage: (a) undamaged case and (b) damaged case.

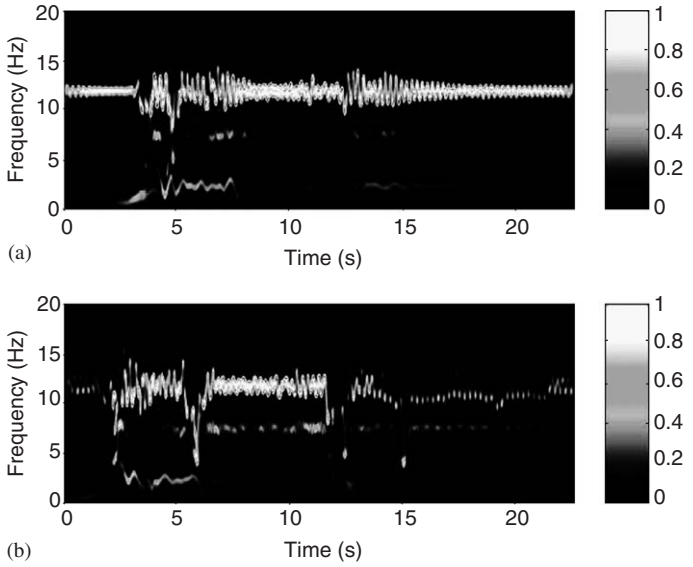

Fig. 23. Second floor acceleration for ground floor damage: (a) undamaged case and (b) damaged case.

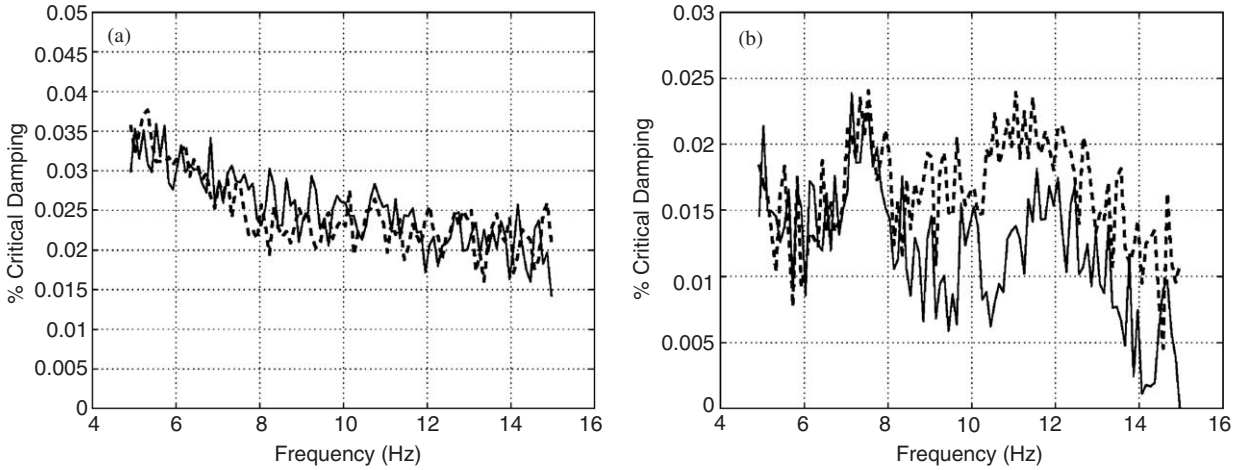

Fig. 24. Time-averaged damping in ground and second floor acceleration responses: ——, undamaged; – –, damaged; (a) ground floor and (b) second floor.

essentially reduce the intensity of the high-frequency band of vibration. This increase in damping is evident in the marginal damping spectrum for the third floor vibration signals displayed in Fig. 27.

For comparison with more familiar wavelet analysis, the same data used in Fig. 25 as an example case study were processed using the standard Morlet wavelet and the results are displayed in Fig. 28. Although some similar features can be seen in Figs. 25 and 28, the differences observed using these two methods are significant. Compared with the Hilbert spectrum, $H(f,t)$, the average overall time–frequency resolution produced by the wavelet is poor. In the Hilbert spectrum plot, the spectrum displays three distinct frequency bands. These frequencies can be identified using simple undamaged model of the structure and were determined to be 2.5, 7, and 12 Hz, respectively, for the first three modes. The Hilbert spectrum also shows the detailed structural response changes as a function of time and frequency. If one uses standard image smoothing techniques, such as applying a 2-D Gaussian filter multiple times, the plots in Fig. 25 can be made to look almost identical to Fig. 28. In this case, some potential important time–frequency information of $H(f,t)$ is being lost and the result approaches the wavelet spectrum.

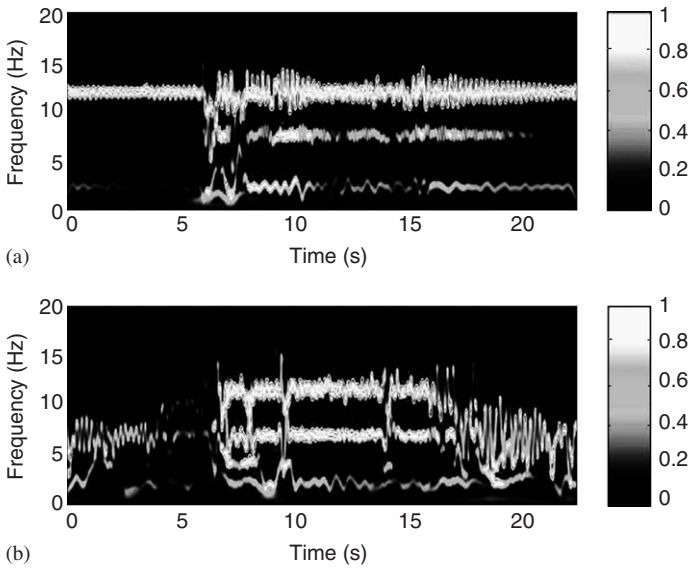

Fig. 25. Second floor acceleration for third floor damage: (a) undamaged case and (b) damaged case.

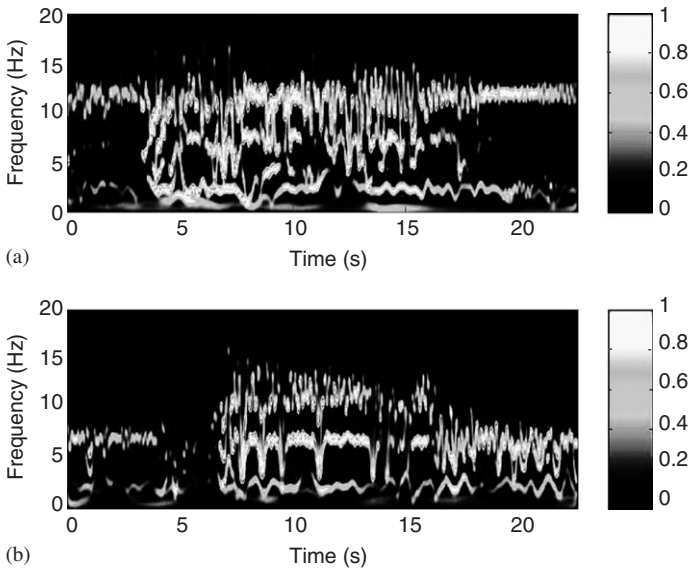

Fig. 26. Third floor acceleration for third floor damage: (a) undamaged case and (b) damaged case.

6.2. Relative Hilbert phase response using EMD

While the use of the intrinsic mode functions coupled with the Hilbert–Huang spectrum and damping analysis provides a wealth of information about the nature of the vibration response, an alternative approach is to process the intrinsic mode functions in such a way that the relative phase between successive degrees of freedom can be used as a metric to infer the location and relative amount of structural damage. Thus, rather than tracking how individual characteristic frequencies change as a result of damage, one can simply track properties associated with the reverberated/dereverberated time-domain response of the signal. As previously

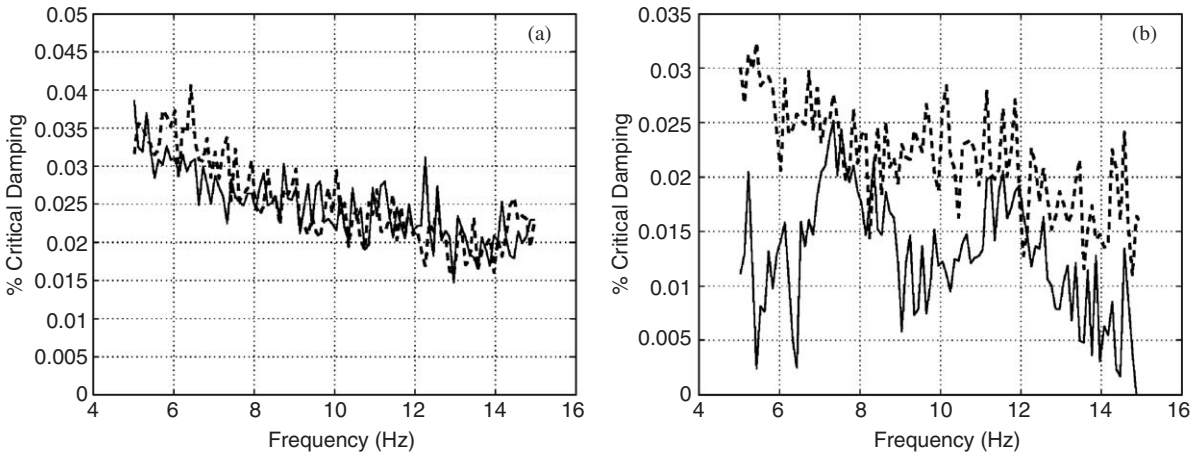

Fig. 27. Time-averaged damping in ground and third floor acceleration responses: ——, undamaged; – –, damaged; (a) ground floor and (b) third floor.

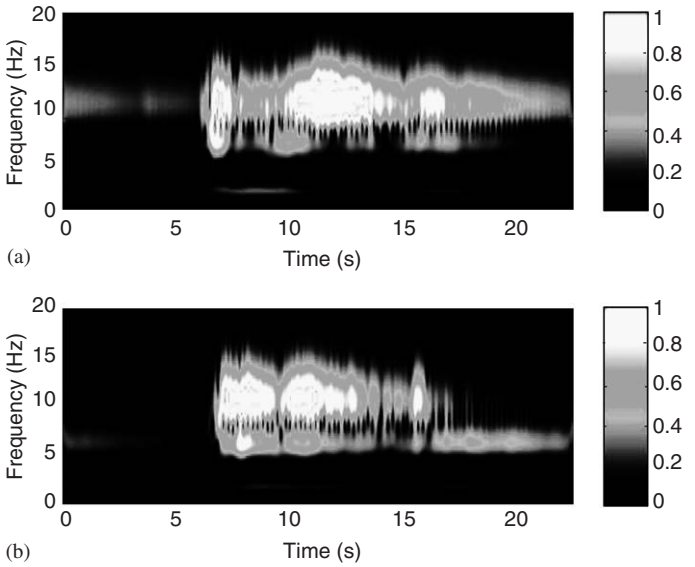

Fig. 28. Morlet wavelet analysis of the second floor acceleration for third floor damage case: (a) undamaged case and (b) damaged case.

shown, the dereverberated phase and the reverberated phase can be used as an indicator of damage when incident energy is initiated from one direction. Using EMD the phase response of each degree of freedom can easily be obtained from the analysis of intrinsic mode functions. Fig. 29 plots the relative phase between successive degrees of freedom for the ground floor damage case described earlier. Results indicate that in the case of ground floor damage the relative phase error shows up in all vibration signals from each floor, suggesting that the damage must have occurred between the ground and first floor. Similarly, in the case of damage in the top floor, Fig. 30 indicates that the relative phase error between the ground and floor, and the first and second floor are unchanged. However, the relative phase error between the second and third floor shows a significant increase, suggesting that the damage is between the second and third floor. Quantifying the amount of structural damage present in the structure requires correlating these relative phase errors with a known value of the stiffness between each degree of freedom. This has been illustrated in earlier work by Ma and Pines [21] where control theory is used to enhance the ability to detect, locate and quantify damage.

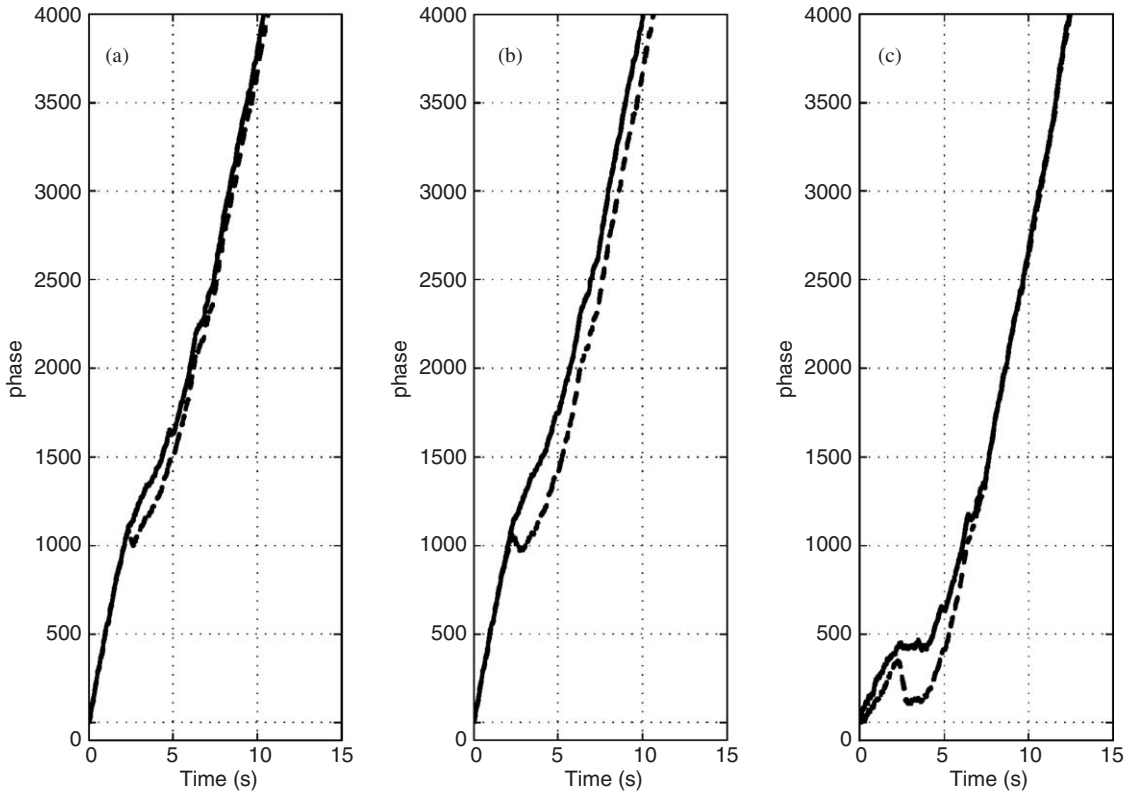

Fig. 29. Damage in ground floor: ——, undamaged; – –, damaged; (a) first floor, (b) second floor and (c) third floor.

As we point out in Section 6.1.1 that the IMFs, shown in Fig. 21, by themselves are difficult to ascertain the presence of damage. More importantly, many of the variations in individual modes are due to computational process. However, when these IMFs are used as a basis function set to compute time–frequency distributions such as the Hilbert spectrum, the presence of structural damage can be easily interpreted. See, for example, discussions of comparing undamaged and damage signal of the second floor for ground floor damage case shown in Fig. 23. Moreover, the relative Hilbert phase damage indicator seems to be even less influenced by the individual IMF variations. The only significant changes in the relative phase, Figs. 29 and 30, are due to structural damage.

7. Summary

In summary, the empirical mode decomposition coupled with the Hilbert–Huang Transform is a powerful new time–frequency signal processing tool that appears to provide finer details about the underlying vibration signals in structures with and without damage. Moreover, when the concept of an intrinsic mode function is coupled with the concept of the phase of a time-domain signal, this information can be used to determine the relative phase response between two successive degrees of freedom. It is this information that allows one to interpret the vibration signal as a wave response traversing discrete structural elements. As these structural elements become damaged, the nature of the wave response changes resulting in phase errors between successive degrees of freedom. The EMD approach has been used to uncover this phase relationship and couple it to the concept of structural damage. Results on a laboratory experimental structure are promising and permit one to determine the presence and location and ultimately the amount of damage with respect to some baseline condition of the structure.

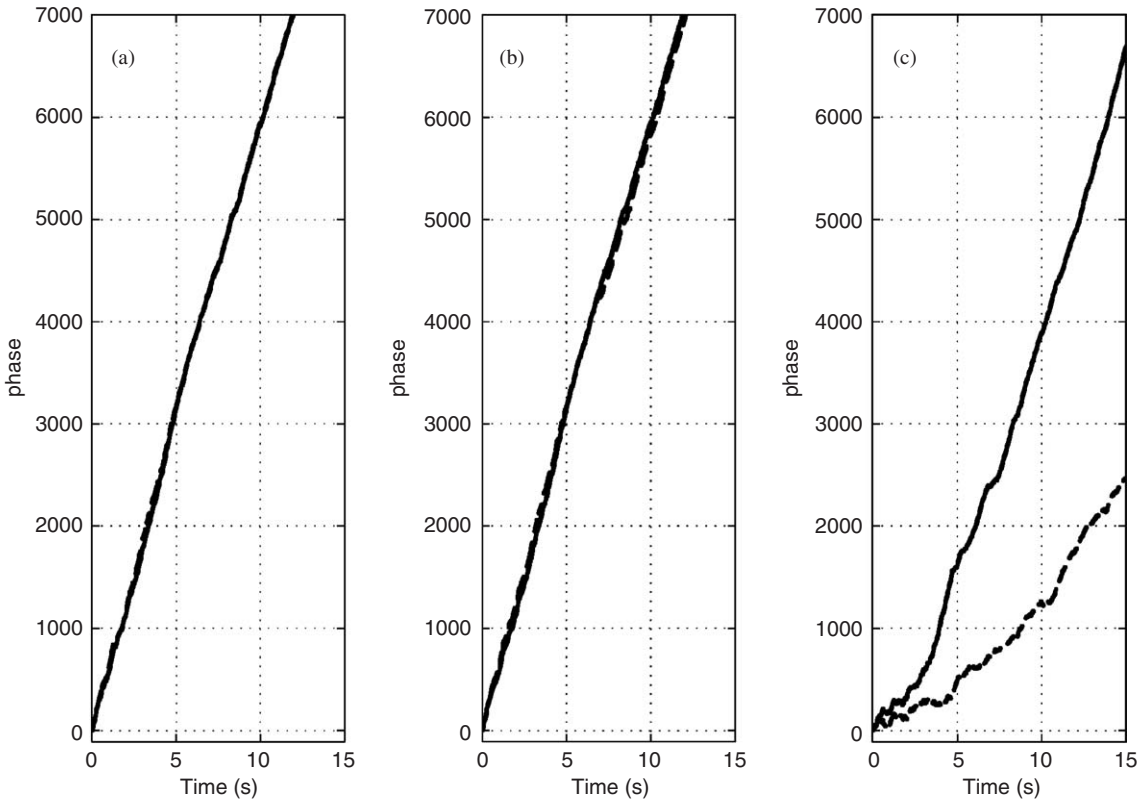

Fig. 30. Damage in third floor: ——, undamaged; – –, damaged; (a) first floor, (b) second floor and (c) third floor.

This approach is extended through experimental demonstrations to a more generalized 2-D structure with damages in multiple locations [22]. In addition, a more recent study has shown that this approach can be applied to data measured from an underwater explosive experiment to detect large composite T-joint structural damage due to shock [23].

References

[1] S.W. Doebling, C.R. Farrar, M.B. Prime, D.W. Shevitz, A review of damage identification methods that examine changes in dynamic properties, *Shock and Vibration Digest* 30 (2) (1998).
[2] N.E. Huang, Z. Shen, S.R. Long, M.C. Wu, H.H. Shih, Q. Zheng, N.-C. Yen, C.C. Tung, H.H. Liu, The empirical mode decomposition and the Hilbert spectrum for nonlinear and non-stationary time series analysis, *Proceedings of the Royal Society of London* 454 (1998) 903–995.
[3] W. Ville, Theorie et applications de la notion de signal analytique, in: *Cables et Transmission*, Vol. 2a, 1948, pp. 61–74 (Translated into English by I. Selin, RAND Corp. Report T-92, Santa Monica, CA, August 1958).
[4] A. Haar, Zur theorie der orthogonalen funktionensystemes, *Mathemathische Annalen* 69 (1910) 331–371.
[5] D. Gabor, Theory of communication, *Journal of the Institution of Electrical Engineers* 93 (1946).
[6] I. Daubechies, Time–frequency localization operators: a geometric phase space approach, *IEEE Transactions on Information Theory* 34 (1988) 605–612.
[7] I. Daubechies, The wavelet transform, time–frequency localization and signal analysis, *IEEE Transactions on Information Theory* 36 (5) (1990) 961–1005.
[8] S.G. Mallat, A theory for multiresolution signal decomposition: the wavelet representation, *IEEE Transactions on Pattern Analysis and Machine Intelligence* 11 (7) (1989) 674–693.
[9] D.E. Newland, Wavelet analysis of vibration, Part I: theory, *Journal of Vibration and Acoustics* 116 (1994) 409–416.
[10] D.E. Newland, Wavelet analysis of vibration, Part, II: wavelet maps, *Journal of Vibration and Acoustics* 116 (1994) 417–425.

[11] S. Mallat, Z. Zhang, Matching pursuit with time–frequency dictionaries, *IEEE Transactions on Signal Processing* 41 (1993) 3397–3415.
[12] S. Jaggi, W.C. Karl, S. Mallat, A.S. Willsky, High resolution pursuit for feature extraction, Technical Report, MIT, November 1995.
[13] S.S. Chen, D.L. Donoho, M.A. Saunders, Atomic decomposition by basis pursuit, *SIAM Journal on Scientific Computing* 20 (1) (1998) 33–61.
[14] W. Sweldens, The lifting scheme: a custom-design construction of biorthogonal wavelets, Technical Report 1994:7, Industrial Mathematics Initiative, Department of Mathematics, University of South Carolina, 1994.
[15] W. Trappe, K.J.R. Liu, Adaptivity in the lifting scheme, in: *Proceedings of the Conference on Information Sciences and Systems*, Baltimore, Maryland, March, 1999, pp. 950–955.
[16] R.L. Claypoole, R.G. Baraniuk, R.D. Nowak, Adaptive wavelet transforms via lifting, in: *Proceedings of the IEEE Conference on Acoustics, Speech, and Signal Processing*, Vol. 3, Seattle, Washington, May 1998, pp. 1513–1516.
[17] P. Samuel, D. Pines, Planetary gearbox diagnostics using adaptive vibration signal representations, in: *American Helicopter Society 57th Annual Forum*, Virginia Beach, Virginia, May 9–11, 2001.
[18] L. Salvino, Empirical mode analysis of structural response and damping, in: *Proceedings of the 18th IMAC*, February 2000.
[19] L. Salvino, Evaluation of structural response and damping using empirical mode analysis and HHT, in: *SCI 2001/ISAS 2001 Proceedings*, Orlando, FL, July 2001.
[20] J. Ma, D.J. Pines, The concept of dereverberation and its application to damage detection in structures, *AIAA Journal* 39 (5) (2001) 111–121.
[21] J. Ma, D.J. Pines, Detecting damage in a building structure model under seismic excitation using dereverberated wave mechanics, *Engineering Structures* 25 (3) (2003) 385–396.
[22] L. Salvino, D.J. Pines, M. Todd, J. Nichols, EMD and instantaneous phase detection of structural damage, in: N. Huang, S. Shen (Eds.), *Hilbert– Huang Transform: Introduction and Applications*, World Scientific, Singapore, 2004.
[23] L. Salvino, E. Rasmussen, D.J. Pines, Detecting structural damage using adaptive feature extraction from transient signals, in: *Proceedings of the Ninth Annual SPIE NDE for Health Monitoring and Diagnostics Conference*, March 2004.